Vol. 08, No. 3 (2026) 1643-1652, doi: 10.24874/PES08.03.019

Proceedings on Engineering Sciences

www.pesjournal.net

FINITE ELEMENT ANALYSIS OF BENDING, CONTACT, AND DYNAMIC BEHAVIOUR OF NON-SYMMETRIC SPUR GEARS

Puttaswamy Srinivasa
Chandrappa Shashishekar
Goud Mallesh[3]

Received 26.05.2026
Revised 05.07.2026
Accepted 26.08.2026

Keywords:

Non-symmetric spur gear, Finite element analysis, Drive side pressure angle, Bending stress, Contact stress, Dynamic analysis, Heavy-duty gears

A B S T R A C T

Non-symmetric spur gears have potential for improving the load carrying capability of gear systems used in mining and metal processing equipment subjected to high and fluctuating loads. This study investigates the bending, contact, and dynamic stress behaviour of standard and non- symmetric spur gears with varying drive side pressure angles using parametric geometry generation and ANSYS finite element analysis (FEA). The Python based involute profile generation showed root thickness deviations below 1.5%, while static FEA results agreed with Tobe's analytical method within 1.7%. Increasing the drive side pressure angle from 20° to 35° reduced bending stress from 66.06 to 47.14 MPa (28.6%). Contact stress decreased from 725.006 MPa to 634.59 MPa, a reduction of 12.47%, reflecting a significant decrease in Von Mises stress at the contact region. Transient analysis showed reductions of 8% in peak bending stress and 24.3% in dynamic contact stress at HPSTC. The results demonstrate that non-symmetric spur gear profiles with increased drive side pressure angles can reduce bending and contact stresses under static and dynamic loading, indicating improved tooth strength and load carrying potential.

© 2026 Published by Faculty of Engineering

1. INTRODUCTION

Mining and metal processing equipment operates under severe mechanical conditions involving high loads, fluctuating torque, shock loading, abrasive contamination, and variable operating speeds. Gear transmission systems used in such applications are exposed to demanding loading conditions that can significantly affect their reliability and durability (Xiong et al., 2026). Consequently, improving gear strength and reliability is essential for ensuring continuous operation and reducing maintenance and downtime in heavy duty industrial applications.

Spur gears are widely employed in industrial power-transmission systems because of their simple geometry, constant velocity ratio, high transmission efficiency, and ease of manufacture. Conventional involute spur gears generally employ symmetric tooth profiles, although the loading and meshing conditions on the drive and coast flanks are inherently different (Kapelevich, 2000). In many applications, gear systems operate predominantly under unidirectional loading, resulting in substantially higher loading on the drive flank than on the coast flank (Karpat et al., 2008; Thomas et al., 2019). Under such

[1] Corresponding author: Goud Mallesh
Email: mallesh@sjce.ac.in

operating conditions, non-symmetric tooth profiles provide an opportunity to tailor the drive and coast flanks independently, thereby improving drive side load carrying capacity and making more effective use of the available tooth material (Kumar et al., 2008; Marimuthu & Muthuveerappan, 2014).

The principal failure mechanisms in heavily loaded gears are tooth root bending and tooth flank contact fatigue. Bending failure is associated with cyclic stresses near the tooth root, whereas repeated Hertzian contact stresses can initiate surface damage such as pitting and spalling (Fernandes, 1996; Fernandes & McDuling, 1997). Classical approaches, including the Lewis bending equation, Hertzian contact theory, and standardized AGMA and ISO formulations, are commonly used to evaluate gear bending and contact stresses (Lisle et al., 2019). However, these analytical approaches may not completely capture local stress concentrations, detailed tooth root geometry, nonlinear contact behaviour, and the actual stress distribution within modified gear profiles (Wen et al., 2018).

The operating environment further increases the possibility of gear degradation. Lubrication deterioration and abrasive contamination can accelerate gear wear and surface damage, particularly in dusty and harsh environments (Mao et al., 2023). Shaft misalignment can produce nonuniform tooth contact and promote scuffing and other gear failures (Kumar & Hirani, 2021). These factors highlight the need for gear geometries capable of providing improved load carrying performance under severe operating conditions.

Non-symmetric spur gears have therefore been investigated as an alternative to conventional symmetric gears. In non-symmetric gears, different pressure angles are employed on the drive and coast flanks, allowing the heavily loaded drive flank to be strengthened while reducing material on the lightly loaded coast flank. Increasing the drive-side pressure angle can increase the tooth-root section and consequently reduce bending stress, while profile shifting can further modify tooth thickness and contact characteristics (Toman & Abdullah, 2020).

Finite element analysis (FEA) has become an important numerical technique for evaluating gear stresses, as it provides detailed information on tooth-root stress concentration, contact-pressure distribution, and stress response under static and dynamic loading (Mallesh et al., 2009a; Puneeth & Mallesh, 2021). Previous investigations have demonstrated that modifications in pressure angle, tooth profile, and gear geometry can significantly influence the bending and contact behaviour of non-symmetric spur gears (Mallesh et al., 2009b). Such numerical approaches are particularly useful for evaluating non-symmetric gear geometries, where local stress distributions and contact behaviour may not be fully represented by conventional analytical formulations.

Although several studies have examined non-symmetric gear geometry, bending strength, contact behaviour, and dynamic response, these aspects have frequently been investigated separately. In particular, studies combining parametric non-symmetric gear generation with static bending analysis, contact-stress evaluation, and transient dynamic analysis for heavy-duty mining and metal-processing applications remain limited. Therefore, the present study investigates the bending, contact, and dynamic stress behaviour of standard and non-symmetric spur gears using parametric geometry generation and ANSYS-based finite element analysis (Zhao et al., 2014). The numerical results are compared with established analytical approaches to assess the influence of drive-side pressure angle on gear stress behaviour.

2. GEAR TOOTH GEOMETRY AND DESIGN PARAMETERS

Mining conveyor systems are critical components in bulk material handling operations. They transport ores, coal, and processed minerals continuously over long distances under heavy load conditions. The gearboxes driving these conveyors operate continuously in dusty and abrasive environments, subjected to high torque, moderate speeds, shock, and impact loading (Vasic et al., 2020). Failure of the gearbox leads to significant production downtime and economic loss. Therefore, estimating the bending, contact, and dynamic stresses developed during operation is crucial for improving the bending resistance of spur gears used in such systems.

For this study, a single stage reduction unit transmitting power from an electric motor to a conveyor drive drum was selected. The chosen design parameters are illustrated in Table 1.

Table 1. Gear design parameters (Botto et al., 2003)

Number of teeth on Pinion/Gear		20/60
Pressure angle	Standard gear	$20^0/20^0$
	non-symmetric gear	$20^0/25^0$
Normal Module, M_n, (mm)		6
Addendum, a (mm)		$1\ M_n$
Dedendum, b (mm)		$1.25\ M_n$
Face width		$10\ M_n$
Speed reduction ratio		3:1
Input speed (motor side, rpm)		980
Conveyor shaft speed, rpm		330
Power transmitted, kw		75

The design parameters presented in Table.1 are used generate tooth profile coordinates using established involute and fillet equations available in the literature (Fetvaci, 2012) for both the standard and non-Symmetric spur gears.

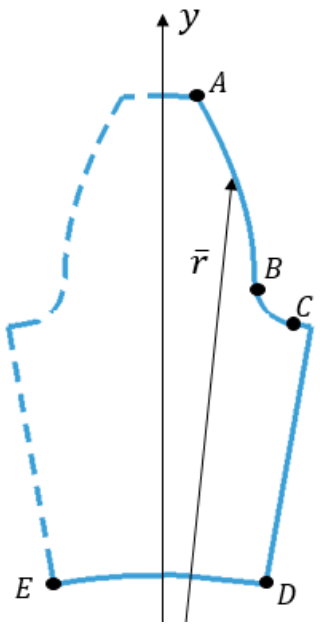


Figure 1. Involute and Fillet Profile

The mathematical formulations used to define the involute curve (AB), fillet curve (BC), and rim thickness region (CD), as illustrated in Figure 1, are applicable to gears generated using standard rack cutter geometry. The cutter parameters required for generating the gear tooth profiles were adopted from the Direct Gear Design (Kapelevich, 2013).

Based on the equations cited in the above reference, a numerical algorithm was developed in Python to generate the two-dimensional tooth profile of both standard and non-symmetric spur gears. The algorithm computes discrete coordinate points corresponding to the involute portion and the root fillet region of the gear tooth using established analytical formulations of involute geometry and rack cutter generation principles.

The computational procedure enables parametric control of key gear parameters such as module, number of teeth, pressure angle, and addendum modification factor. This framework allows systematic variation of the drive-side pressure angle for the development of non-symmetric gears while maintaining geometric compatibility and conjugate action. The overall computational workflow adopted for gear geometry creation is illustrated in Figure 2.

Using the Python-generated output in terms of X and Y coordinate points, the splines, boundary lines, and the area of a single gear tooth both symmetric and non-symmetric were created in the ANSYS Mechanical environment as shown in Figure 3 were developed by varying the pressure angle on drive side.

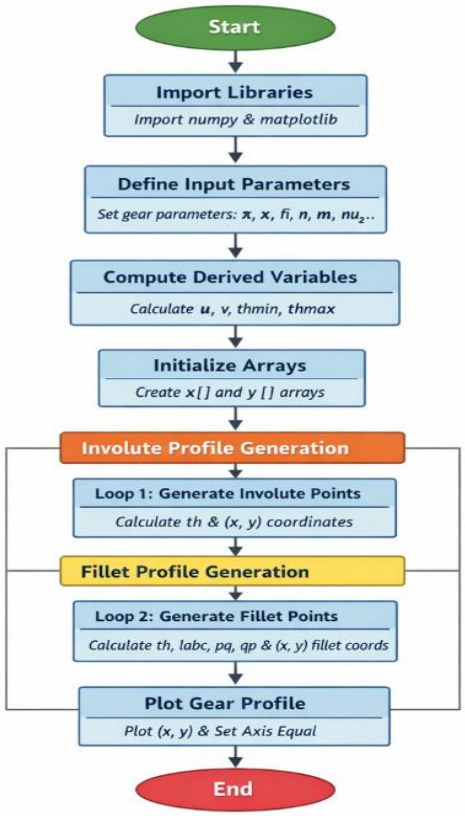


Figure 2. Computational Framework for Spur Gear Geometry Construction

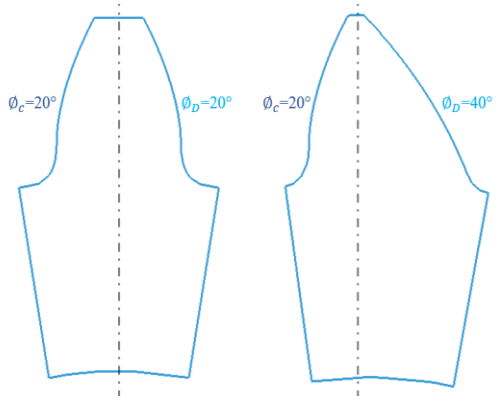


Figure 3. 2-D model of standard and Non-symmetric Gears

3. FINITE ELEMENT ANALYSIS

The reliability and load-carrying capacity of mining gears are primarily determined by the stresses generated during operation. These stresses are generally classified as static, contact, and dynamic stresses, each contributing to different failures. As per established standards, gear static bending stress is evaluated using the Lewis equation as well as the AGMA and ISO standards, given by Equations 1, 2, and 3, respectively.

$$\sigma_b = \frac{F_t}{b\, m\, Y} \tag{1}$$

$$\sigma_{AGMA} = \frac{F_t\, K_o\, K_v\, K_S\, K_m}{(b\; m\; J) \times K_B} \tag{2}$$

$$\sigma_F = \frac{F_t}{(b\; m_n) Y_f Y_S Y_\beta Y_{DT}} \tag{3}$$

Contact stresses developed at the tooth flank are estimated using Hertzian contact theory and AGMA guidelines, given by Equations 4 and 5. In practical operation, gears are also subjected to dynamic effects caused by time-varying mesh stiffness, transmission error, and inertial forces, which increase both bending and contact stresses beyond their static values.

$$\sigma_{cA} = C_p \sqrt{F_t K_o K_v K_s \frac{K_m C_f}{d_p B I}} \tag{4}$$

$$\sigma_{cH} = \sqrt{\frac{F_t\left(1+\frac{R_1}{R_2}\right)}{R_1 B \pi \left[\frac{(1-\vartheta_1^2)}{E_1}+\frac{(1-\vartheta_2^2)}{E_2}\right] \sin\emptyset}} \tag{5}$$

Finite Element Analysis (FEA) is a numerical tool that provides a precise and systematic framework for evaluating spur gear stresses under static, contact, and dynamic conditions, complementing conventional analytical methods (Zienkiewicz et al., 2013). In FEA, the gear geometry is discretized into finite elements connected at nodes, where material properties, boundary conditions, and loads are applied to approximate the true stress and deformation behaviour of the component (Chen & Tsay, 2002). Compared to purely analytical approaches such as the Lewis or AGMA equations, FEA captures localized stress concentrations, complex tooth-root fillet geometry, and non-uniform load distribution more accurately, making it particularly suitable for gears with non-symmetric tooth profiles. In this study, the commercial software ANSYS was used to perform static bending, contact, and dynamic stress analyses of the spur gear models.

The Python-generated X and Y coordinate points of the involute and fillet profiles of the gear teeth are imported into the ANSYS environment using the preprocessor initialization command (/PREP7). Each coordinate pair is defined as a key point (K) in the APDL command format K, key point number, X-coordinate, Y-coordinate, as illustrated by a representative set of profile points shown in Figure 4.

File Edit Format View Help

```
          X          Y
k,1,-1.439468,53.980811
k,2,-1.465023,53.932638
k,3,-1.490386,53.884588
k,4,-1.515559,53.836661
```

Figure 4. Sample X–Y key point coordinates generated in Python

These key points are then used to generate splines along the involute flank and fillet regions, along with boundary lines, and are subsequently used to create the area of a single tooth, three teeth, or the whole gear body for both standard and non-symmetric gears, as illustrated in Figure 5.

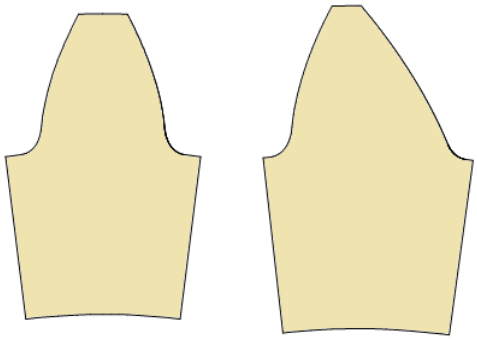


Figure 5. Tooth profile geometry generated for standard and non-symmetric gears

The resulting 2D gear tooth model is discretized into a finite element mesh using 8-noded quadrilateral elements, with a finer mesh density applied in the fillet and tooth-contact regions to accurately capture the localized stress gradients in these critical zones. Based on the transmitted power and rotational speed, the tangential tooth load is calculated and applied at the Highest Point of Single Tooth Contact (HPSTC), consistent with AGMA and ISO loading conventions. Boundary conditions are imposed by constraining the two radial lines and the inner rim surface, representing the shaft-mounting condition, as shown in Figure 6. The gears are modelled using steel material properties, with a Young's modulus of 210 GPa and a Poisson's ratio of 0.3, to represent realistic material behaviour for accurate bending and contact stress evaluation.

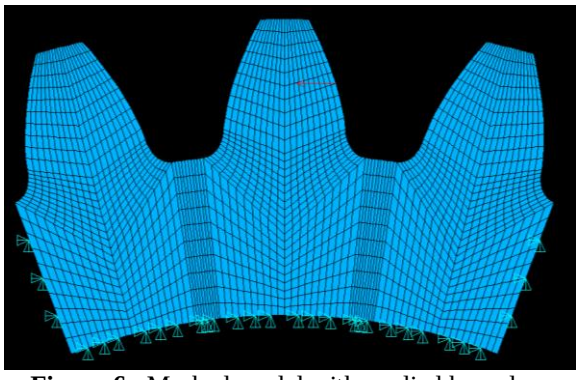


Figure 6. Meshed model with applied boundary conditions

A 2D contact analysis was performed in ANSYS to estimate the Hertzian contact stresses and contact forces at the gear tooth interface. Linear elastic isotropic material properties, as specified in the preceding section, were assigned to both the pinion and gear bodies. A torque corresponding to 75 kW was applied at the pinion bore, while the gear bore was fully constrained. A surface-to-surface contact pair was defined at the mating tooth flanks using the augmented Lagrangian algorithm,

with the convex flank designated as the contact surface and the mating flank as the target surface (Vijayarangan & Ganesan, 1994). The mesh was progressively refined at the contact zone, as shown in Figure 7, to accurately capture the steep stress gradients inherent to Hertzian contact.

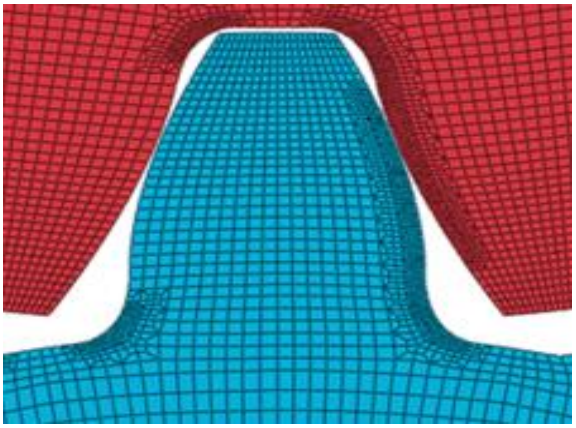


Figure 7. Gear pair contact configuration for stress analysis

Transient dynamic analysis of a standard spur gear tooth was performed using ANSYS to investigate the time-varying contact stress and dynamic response under realistic meshing conditions (Zou et al., 2020). The full transient method, employing the Newmark time integration scheme, was used to solve the complete equation of motion, thereby accounting for the effects of inertia, damping, and time-dependent contact forces throughout the meshing cycle. A surface-to-surface contact pair was defined at the mating tooth flanks using the augmented Lagrange algorithm, which ensures accurate enforcement of the contact constraints while improving convergence stability. A time-varying torque was applied at the gear center to simulate realistic dynamic meshing conditions and capture the fluctuations in contact stress as the gear teeth engaged and disengaged. A similar transient dynamic analysis was subsequently carried out using ANSYS for a non-symmetric gear, in order to compare its contact stress distribution and dynamic response characteristics with those of the standard gear tooth.

4. RESULTS AND DISCUSSIONS

This section presents the results obtained from the geometric modelling, analytical calculations, and finite element simulations carried out on the standard spur gear tooth. The discussion is organized into four parts, each building progressively from geometric validation through static and contact stress analysis to the final dynamic response under realistic meshing conditions.

First, the spur gear tooth geometry generated using a Python-based parametric script is presented, and the accuracy of the involute profile construction is validated against standard gear design parameters to ensure that the model faithfully represents true involute tooth geometry before proceeding to further analysis. Second, the static bending stress results obtained from ANSYS finite element analysis (FEA) are discussed and compared with analytical predictions derived from the AGMA bending stress equation, the ISO 6336 standard, and the classical Lewis form factor method, thereby establishing confidence in the finite element model through cross-validation with well-established analytical approaches. Third, the contact stress distribution at the mating tooth flanks is evaluated using ANSYS and validated against Hertz contact theory, providing insight into the localized stress concentration that occurs at the point of tooth engagement. Finally, the dynamic contact stress response obtained from the transient dynamic analysis in ANSYS is presented, highlighting the influence of inertia and time-varying meshing forces on the stress distribution across the gear tooth surface, and illustrating how the stress behavior under dynamic conditions differs from that predicted by static and quasi-static approaches.

4.1 Geometry and static bending stress analysis

The gear tooth geometry was generated parametrically using a Python-based script, following standard involute profile construction. The addendum tooth thickness was maintained at 0.2 times the normal module to ensure adequate tip strength (Radzevich, 2016). Root thickness at the critical section, the location most susceptible to bending failure, was evaluated and compared with established analytical methods (Mallesh et al., 2009c), as summarized in Table 2.

The computed values show close agreement with literature across the 20°–30° pressure angle range, with a marginally higher deviation at lower angles that diminishes as the pressure angle increases. This trend is consistent with the higher root thickness, and correspondingly greater load-carrying capacity, associated with larger pressure angles. Beyond 42°, however, the addendum tip becomes excessively sharp, increasing susceptibility to localized failure under contact loading.

Table 2. Comparison of Critical Section Tooth Thickness

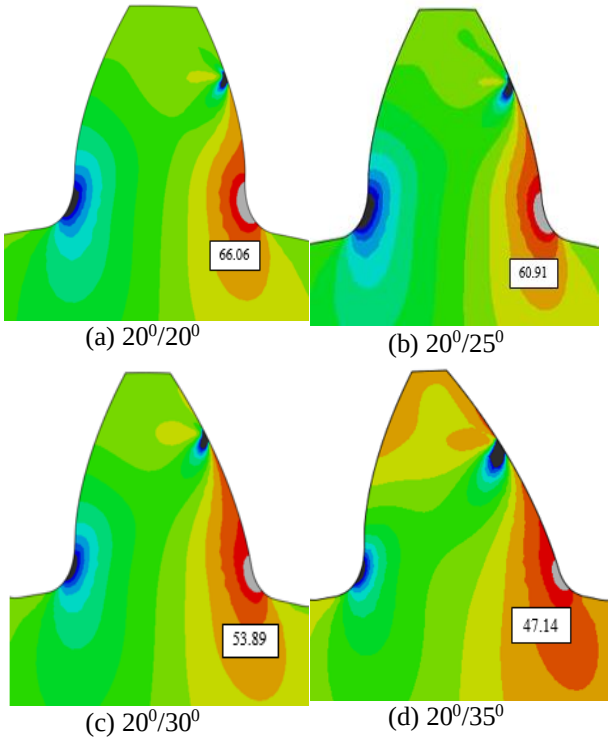
Drive side Pressure angle, (°)	Tooth thickness at the Critical Section, mm	
	Python Script	Literature
20	5.8689	5.7858
25	6.1350	6.0809
30	6.4281	6.4134

Table 3 and Figure 8 present the static bending stress distribution obtained for symmetric and non-symmetric spur gears. The results indicate that increasing the drive-side pressure angle reduces stress concentration at the critical section by shifting the location of peak stress away from the root fillet and toward the rim, an effect attributed to the corresponding increase in root thickness at higher pressure angles.

Table 3. Comparison of Bending Stress: FEA and Analytical Approaches

Drive side Pressure angle, (°)	Bending stress at the tooth root, MPa	
	(Deng, et al., 2003)	FEM
20	64.95	66.06
25	61.95	60.91
30	55.50	53.89
35	48.75	47.14

Symmetric gears exhibit higher stress concentration at the tooth root due to the identical loading conditions on both the drive and coast sides, whereas non-symmetric gears demonstrate a more uniform stress distribution across the tooth profile, thereby reducing the risk of localized failure.



(a) $20^0/20^0$ (b) $20^0/25^0$

(c) $20^0/30^0$ (d) $20^0/35^0$

Figure 8. Bending stress contours for (a) 20°/20°, (b) 20°/25°, (c) 20°/30°, and (d) 20°/35° pressure angle combinations

Furthermore, an increase in the drive-side pressure angle enhances root thickness and, consequently, load-carrying capacity, confirming the effectiveness of non-symmetric gear designs in improving bending strength. The results obtained from finite element modelling (FEM) using ANSYS and the analytical calculations based on (Deng, et al., 2003) are in good agreement, further validating the accuracy of the finite element model.

4.2 Hertz contact stress.

For standard spur gear teeth, contact stress was estimated using AGMA, Hertzian contact theory, and FEA. As shown in Table 4, the difference between the two theoretical methods (AGMA and Hertzian) is negligible, while the discrepancy between the theoretical and FEA results is approximately 4-5%. This variation can be attributed to the friction coefficient used in the contact algorithm, the sharp variation of Hertzian contact stress near the contact point, the shifting contact point during meshing, and the finite element size in the contact zone.

Table 4. Contact stress for symmetric spur gears

Method	Contact Stress, MPa
AGMA	695.165
Hertz	696.592
FEA (ANSYS)	725.006

No standardized method is currently available for evaluating contact stress in non-symmetric spur gears. Therefore, FEA using ANSYS, with refined meshing in the contact regions, was adopted as the preferred approach for calculating contact stress in these gears. As evident from Table 5, an increase in drive-side pressure angle reduces sliding velocity and, correspondingly, the contact stress. The contact stress decreases from 725.006 MPa at 20°/20° to 634.59 MPa at 20°/35°, a reduction of approximately 12.47% with increasing drive-side pressure angle.

Table 5. Contact stress for non-symmetric gears.

Drive side Pressure angle, (°)	Contact stress, MPa
20	725.006
25	707.94
30	693.18
35	634.59

Contact stress results evaluated using ANSYS are consistent with those reported for non-symmetric spur gears, where a 15–25% reduction in contact stress was attributed to improved contact curvature (Toman & Abdullah, 2024). Similarly, the observed reduction in sliding velocity corroborates the kinematic behavior of non-symmetric gear tooth profiles established in the literature (Zhang et al., 2020; Costopoulos & Spitas, 2009). These findings confirm that non-symmetric gear tooth geometry with an optimized pressure angle effectively reduces contact stress and enhances surface durability.

Figure 9 presents the Von Mises stress distribution in the contact region. The results indicate a progressive decrease in stress with increasing pressure angle. Among the investigated configurations, the maximum Von Mises stress of 294.071 MPa is observed for the 20°/30° pressure angle combination. In all cases, the maximum stress remains below the material yield strength of 310 MPa, indicating that the gear teeth remain within the elastic range under the applied loading conditions. Furthermore, the stress magnitude decreases progressively with increasing distance from the contact zone, which is consistent with the localized nature of the Hertzian contact stress distribution.

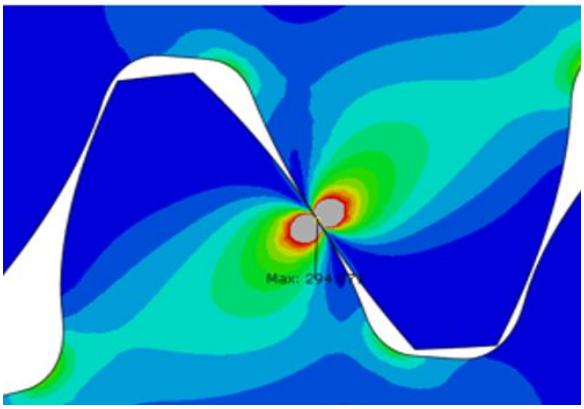


Figure 9. Von mises stress at the contact region for non-symmetric gear

4.3 Dynamic bending and contact stress

Figure 10 shows the dynamic bending stress at the fillet region for standard and non-symmetric spur gear tooth profiles. The maximum bending stress for the 20°/20° pair is 69.8 MPa at t = 0.0175 s, while the 20°/30° pair yields a reduced peak of 64.2 MPa at t = 0.0137 s, a reduction of approximately 8%. In both cases, the stress rises sharply at tooth engagement, peaks at single-tooth contact, and decays rapidly after disengagement, followed by low-amplitude residual oscillations that indicate dynamic load fluctuations. These minor secondary peaks confirm the presence of residual bending stresses, which are identified as primary contributors to fatigue damage accumulation. The results indicate that the non-symmetric tooth profile effectively reduces dynamic bending stress at the critical fillet section, a trend expected to be favorable for gear fatigue life under dynamic operating conditions.

Figure 11 presents the effective Von Mises stress distributions at the contact region which decreases from 359.820 MPa to 271.85 MPa as the drive-side pressure angle increases from 20° to 35°, a reduction of approximately 24.44%. This reduction is attributed to the increased radius of curvature of the involute profile, which reduces both the Hertzian contact half-width and the sliding velocity at the contact interface.

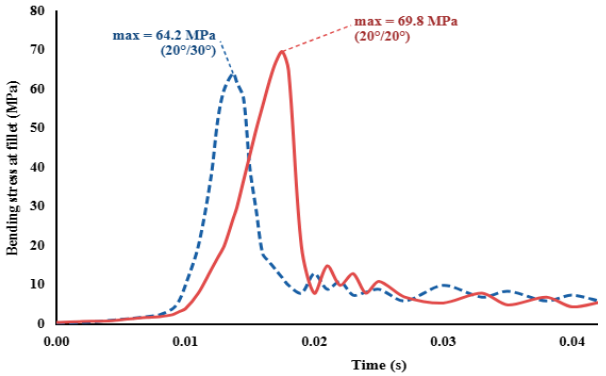


Figure 10. Dynamic bending stress at the fillet region for standard and non-symmetric spur gear tooth profiles

The HPSTC location shifts progressively from the root toward the tip of the tooth flank with increasing pressure angle, consistent with the modified tooth geometry described by Litvin. The effective stress contours confirm a corresponding reduction at the contact zone and root fillet region, from 359.82 MPa (20°/20°) to 271.85 MPa (20°/35°), reflecting the combined benefit of reduced contact stress and improved load distribution across the tooth flank.

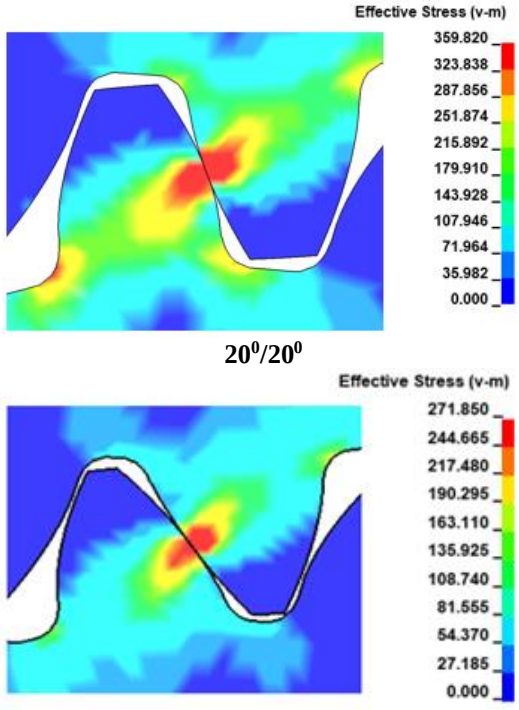


Figure 11. Effective Von Mises stress distribution at the HPSTC

5. CONCLUSION

This study investigated bending stress, contact stress, and dynamic stress behavior in standard and non-symmetric spur gears using parametric geometry generation and ANSYS FEA. The Python-based involute profile script showed close agreement with reference data, with root thickness deviations below 1.5% across the 20°–30° pressure angle range. Static FEA results correlated well with Tobe's analytical method, with deviations within 1.7%. Increasing the drive-side pressure angle from 20° to 35° reduced bending stress from 66.06 MPa to 47.14 MPa, a reduction of 28.6%. For standard gears, contact stress results from AGMA (695.165 MPa), Hertzian theory (696.592 MPa), and FEA (725.006 MPa) agreed within 4.3%. For non-symmetric gears, contact stress decreased from 725.006 MPa to 634.59 MPa, a reduction of 12.47%, reflecting a significant decrease in Von Mises stress at the contact region. Transient dynamic analysis showed a reduction in peak bending stress from 69.8 MPa to 64.2 MPa (8%), while dynamic contact stress at the HPSTC decreased from 731.11 MPa to 553.69 MPa (24.3%).

These results confirm that non-symmetric spur gear profiles with optimized pressure angles reduce bending and contact stresses under both static and dynamic loading conditions, thereby improving tooth strength, surface durability, and load-carrying capacity compared to standard symmetric profiles.

References:

Botto, I., Hurtado, E. O., & Lovell, S. S. (2003). Open Gears for the Mining Industry: Material and Manufacturing Process Selection. In *International Design Engineering Technical Conferences and Computers and Information in Engineering Conference* (Vol. 37025, pp. 827-851). https://doi.org/10.1115/DETC2003/PTG-48104

Chen, Y. C., & Tsay, C. B. (2002). Stress analysis of a helical gear set with localized bearing contact. *Finite Elements in Analysis and Design*, *38*(8), 707-723. https://doi.org/10.1016/S0168-874X(01)00100-7.

Costopoulos, T., & Spitas, V. (2009). Reduction of gear fillet stresses by using one-sided involute asymmetric teeth. *Mechanism and Machine Theory*, *44*(8), 1524-1534. https://doi.org/10.1016/j.mechmachtheory.2008.12.002

Deng, G., Nakanishi, T., & Inoue, K. (2003). Bending load capacity enhancement using an asymmetric tooth profile (1st report, influences of pressure angle on tooth root stress and bending stiffness). *JSME International Journal Series C Mechanical Systems, Machine Elements and Manufacturing*, *46*(3), 1171-1177. https://doi.org/10.1299/jsmec.46.1171

Fernandes, P. J. L. (1996). Tooth bending fatigue failures in gears. *Engineering Failure Analysis*, *3*(3), 219-225. https://doi.org/10.1016/1350-6307(96)00008-8

Fernandes, P. J. L., & McDuling, C. (1997). Surface contact fatigue failures in gears. *Engineering Failure Analysis*, *4*(2), 99-107. https://doi.org/10.1016/S1350-6307(97)00006-X

Fetvaci, C. (2012). Computer simulation of involute tooth generation. IntechOpen. https://doi.org/10.5772/34079

Kapelevich, A. (2000). Geometry and design of involute spur gears with asymmetric teeth. *Mechanism and Machine Theory*, *35*(1), 117–130. https://doi.org/10.1016/S0094-114X(99)00002-6

Kapelevich, A. L. (2013). *Direct Gear Design.* CRC Press. https://doi.org/10.1201/b13920

Karpat, F., Ekwaro-Osire, S., Cavdar, K., & Babalik, F. C. (2008). Dynamic analysis of involute spur gears with asymmetric teeth. *International Journal of Mechanical Sciences*, *50*(12), 1598-1610. https://doi.org/10.1016/j.ijmecsci.2008.10.004

Kumar, P., & Hirani, H. (2021). Misalignment effect on gearbox failure: An experimental study. *Measurement*, *169*, 108492. https://doi.org/10.1016/j.measurement.2020.108492

Kumar, V. S., Muni, D. V., & Muthuveerappan, G. (2008). Optimization of asymmetric spur gear drives to improve the bending load capacity. *Mechanism and Machine Theory*, *43*(7), 829-858. https://doi.org/10.1016/j.mechmachtheory.2007.06.006

Lisle, T. J., Shaw, B. A., & Frazer, R. C. (2019). Internal spur gear root bending stress: A comparison of ISO 6336: 1996, ISO 6336: 2006, VDI 2737: 2005, AGMA, ANSYS finite element analysis and strain gauge techniques. *Proceedings of the institution of mechanical engineers, Part C: Journal of Mechanical Engineering Science*, *233*(5), 1713-1720. https://doi.org/10.1177/0954406218774364

Mallesh, G., & Math, V. B. (2009c). Estimation of critical section and bending stress analysis for asymmetric spur gear tooth. In 14th National Conference on Machines and Mechanisms (NaCoMM09), NIT, Durgapur, India (pp. 17-18).

Mallesh, G., Math, V.B., Venkatesh, Shankarmurthy, H.J., Shiva Prasad, P., Aravinda, K (2009b). Parametric analysis of asymmetric spur gear tooth. In: 14th National Conference on Machines and Mechanisms (NaCoMM09), NIT, Durgapur, India, 17–18 Dec 2009, NaCoMM-2009-MMRAIAG16

Mallesh, G., V. B. Math, Prabodh Sai Dutt R. Ashwij, and Rajendra Shanbhag. (2009a). Effect of tooth profile modification in asymmetric spur gear tooth bending stress by finite element analysis. In 14th National Conference on Machines and Mechanisms (NaCoMM09), NIT, Durgapur, India (pp. 17-18).

Mao, Y., Tong, J., Chin, Z. Y., Borghesani, P., & Peng, Z. (2023). Transmission-error-and vibration-based condition monitoring of gear wear with contaminated lubricant. *Wear*, *523*, 204760. https://doi.org/10.1016/j.wear.2023.204760

Marimuthu, P., & Muthuveerappan, G. (2014). Influence of pressure angle on load sharing based stresses in asymmetric normal contact ratio spur gear drives. *Applied Mechanics and Materials*, *465-466*, 1229-1233. https://doi.org/10.4028/www.scientific.net/AMM.465-466.1229

Puneeth, M. L., & Mallesh, G. (2021). Static contact behavior of asymmetric spur gear. *Materials Today: Proceedings*, *47*, 3095-3104.https://doi.org/10.1016/j.matpr.2021.06.076

Radzevich, S. P. (2016). *Dudley's handbook of practical gear design and manufacture.* CRC press.

Thomas, B., Sankaranarayansamy, K., Ramachandra, S., & SP, S. K. (2019). Selection of Pressure Angle based on Dynamic Effects in Asymmetric Spur Gear with Fixed Normal Contact Ratio. *Defence Science Journal*, *69*(3), 303-310. https://doi.org/10.14429/dsj.69.13636

Toman, A. A., & Abdullah, M. Q. (2020). An analytical solution for the maximum tensile stress and stress concentration factor investigations for standard, asymmetric fillets, asymmetric pressure angle and profile shifted helical and spur gears. *Journal of Engineering*, *26*(7), 217-237. https://doi.org/10.31026/j.eng.2020.07.15

Toman, A. A., & Abdullah, M. Q. (2024). An analytical approach for predicting the fillet and contact stresses in symmetric and asymmetric spur gears under frictional mesh assumptions. *Results in Engineering*, *23*, 102391. https://doi.org/10.1016/j.rineng.2024.102391

Vasic, M., Stojanovic, B., & Blagojevic, M. (2020). Fault analysis of gearboxes in open pit mine. *Applied Engineering Letters*, *5*(2), 50-61. https://doi.org/10.18485/aeletters.2020.5.2.3.

Vijayarangan, S., & Ganesan, N. (1994). Static contact stress analysis of a spur gear tooth using the finite element method, including frictional effects. *Computers & structures*, *51*(6), 765-770. https://doi.org/10.1016/S0045-7949(05)80016-1

Wen, Q., Du, Q., & Zhai, X. (2018). A new analytical model to calculate the maximum tooth root stress and critical section location of spur gear. *Mechanism and Machine Theory*, *128*, 275-286. https://doi.org/10.1016/j.mechmachtheory.2018.05.012

Xiong, G., Dong, Q., Ge, Y., Xie, Z., Shi, X., & Huang, W. M. (2026). Damage modeling of gear contact fatigue considering surface property gradients. *International Journal of Fatigue*, *212*, 109799. https://doi.org/10.1016/j.ijfatigue.2026.109799

Zhang, X., Zhou, Q., & Zhang, K. (2020). Analysis of contact strength of asymmetric gear for small diameter turbodrill reducer. Journal of Mechanical Transmission, 44(7), 95–101. doi:10.16578/j.issn.1004.2539.2020.07.016

Zhao, N., Zhang, M. Q., & Guo, H. (2014). Stress analysis of asymmetric spur face-gear pair based on finite element method. *Applied Mechanics and Materials*, *483*, 309-314. https://doi.org/10.4028/www.scientific.net/AMM.483.309

Zienkiewicz, O. C., Taylor, R. L., & Zhu, J. Z. (2013). The finite element method: its basis and fundamentals. Butterworth-Heinemann.

Zou, X., Yang, C., & Liu, B. (2020). The contact and transient dynamic analysis of gear meshing with ANSYS. *Open Access Library Journal*, *7*(9), 1-10. https://dx.doi.org/10.4236/oalib.1106771

Puttaswamy Srinivasa
Siddaganga Institute of Technology,
Department of Mechanical Engineering,
Tumkuru, Karnataka,
India,
psrinivasa87@gmail.com
ORCID 0009-0000-1368-9829

Chandrappa Shashishekar
Siddaganga Institute of Technology,
Department of Mechanical Engineering,
Tumkuru, Karnataka,
India,
csshek@sit.ac.in
ORCID 0000-0003-3013-2795

Goud Mallesh
Sri Jayachamarajendra College of
Engineering, JSS S&T University,
Department of Mechanical Engineering,
Mysuru, Karnataka,
India,
mallesh@sjce.ac.in
ORCID 0000-0002-4113-107X